Optimization of metal dopant effect on ZnO nanoparticles for enhanced visible LED photocatalytic degradation of citalopram: comparative study and application to pharmaceutical cleaning validation

Veronia S. Nazim[1], Ghada M. El-Sayed[1], Sawsan M. Amer[1] and Ahmed H. Nadim[1*]

Abstract

Metal doping is an effective method to tune the optical and chemical properties of nanoparticles. Herein, a comparative study was conducted to assess the effect of metal dopant (Mg, Cu and Sn) on ZnO nanoparticles for visible LED photocatalysis. The photocatalysts were synthesized via a facile co-precipitation method. Doped ZnO nanoparticles were employed for photodegradation of citalopram; a commonly used antidepressant drug. The structural, morphological and optical properties of the nanoparticles were analyzed using high resolution transmission electron microscopy, X-ray diffraction, Brunauer-Emmett-Teller measurements and diffuse reflectance spectroscopy. A decrease in band gap energy was obtained for Mg (3.21 eV), Cu (3.15 eV) and Sn (3.05 eV) compared to undoped ZnO (3.34 eV). Results showed that the photocatalytic activity of ZnO nanoparticles towards citalopram degradation under visible light was enhanced by doping with Sn which showed superior photocatalytic performance compared to Cu. Whereas, Mg doped ZnO demonstrated the lowest photocatalytic activity. Full factorial design (2^4) was conducted to investigate the effect of dopant, pH, catalyst loading and initial citalopram concentration on the efficiency of the treatment process. The interaction between the metal dopant and pH had significant impact on photodegradation efficiency. At optimum conditions, 80% degradation of 25 μg mL^{-1} citalopram was obtained in 2 h using commercially available LED light using 0.5 mg mL^{-1} Sn doped ZnO. Kinetics of citalopram degradation was also investigated and was found to follow pseudo-first order kinetics. The optimized photocatalytic protocol was successfully applied for treatment of water samples obtained from production lines during the cleaning validation cycles of citalopram. Sn and Cu doped ZnO nanoparticles had great sustainability for wastewater treatment as it kept its catalytic behavior up to three cycles without significant decrease in photocatalytic activity. The integration of such an approach into the currently employed cleaning validation protocols would offer an economical advantage for pharmaceutical wastewater treatment.

Keywords ZnO nanoparticles, Metal dopant, Visible light photocatalysis, Pharmaceutical wastewater treatment, Cleaning validation
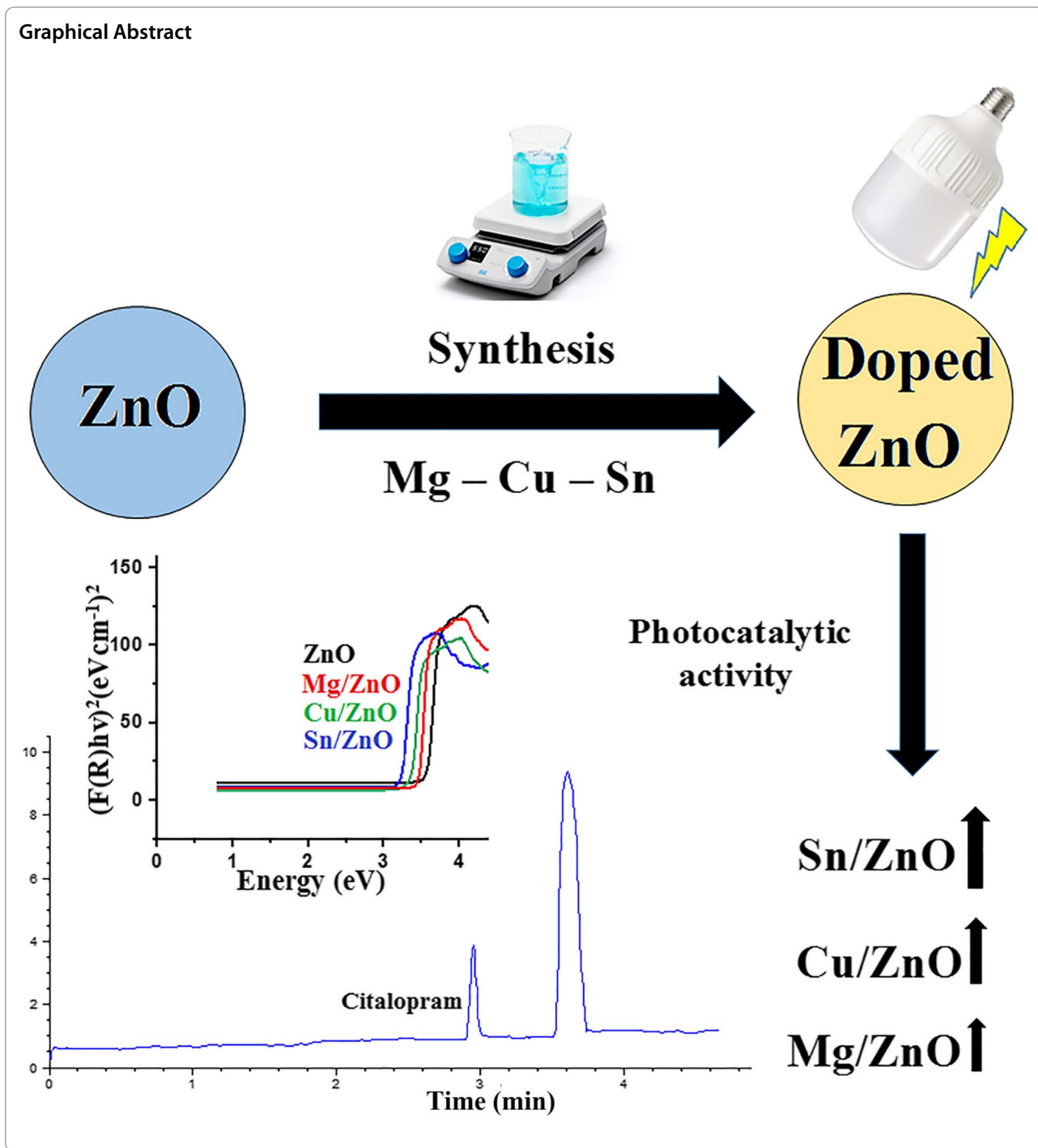
*Correspondence:
Ahmed H. Nadim
ahmed.nagib@pharma.cu.edu.eg
Full list of author information is available at the end of the article

Graphical Abstract

1 Introduction

Recent studies have revealed the presence of many pharmaceutical residues in a wide range of ecosystems [1]. Attention is drawn to avoid undesired accumulation of such compounds in the environment. Proper pharmaceutical wastewater treatment should guard against the presence of complex organic molecules in the aquatic environment [2, 3]. Semiconductor photocatalysis had emerged as one of the most effective means of dealing with wastewater contaminants due to its ability to convert hazardous pollutants into non-toxic chemicals effectively [4]. Also, it is a simple, economic, and ecofriendly technique that can be applied to high complex, low biodegradable, and high concentration of

pollutants. Zinc oxide nanoparticles (ZnO NPs) have been used as an alternative photocatalyst to TiO_2 [5]. They possess similar band gap energy and also strong oxidation ability, chemical stability, biocompatibility, non-toxicity, high photosensitivity and relatively low cost [6]. However, ZnO NPs have shown limited performance in degrading organic pollutants due to their wide band gap that limits their operational range to the ultraviolet region that accounts for less than 5% of the solar spectrum. Moreover, their relatively fast rate of recombination of photo-induced electron hole pairs is a challenge that results in low photodegradation efficiency [7]. Therefore, efforts are directed to decrease the band gap energy to enhance visible light absorption thus minimizing energy cost for large scale wastewater treatment [8, 9], thus minimizing energy cost for large scale wastewater treatment [10]. Development of visible light active ZnO NPs can be achieved by different approaches such as surface modification via dye sensitization [11], coupling with a narrow band gap semiconductor [12] as well as metal and nonmetal doping [6]. Metal doping had proved to be a successful approach for obtaining photocatalysts with improved photonic efficiencies using less than 10% of foreign cations for modifying the semiconductor. The proper dopants could act as traps to increase the separation of charged carriers and inhibit the recombination of photogenerated electron hole pairs. With this strategy, it is possible to shift the optical response towards higher wavelengths and to hinder electron–hole recombination, increasing the photoactivity under visible light irradiation. Various methods have been developed for the synthesis of metal doped ZnO NPs including chemical vapour deposition, physical evaporation, laser ablation and solvo-thermal processes [13, 14]. However, these methods are often associated with several drawbacks such as tedious procedures, various hazardous chemicals, difficulty in removing solvents and precursors used, as well as in maintaining the uniformity of NPs. Co-precipitation is considered an attractive method for photocatalyst preparation at the industrial scale owing to its short reaction time, low reaction temperature and the absence of solid wastes [15]. In addition, the type of dopant used is a critical factor in determining the overall activity of the photocatalysts. Three metals Mg, Cu and Sn were particularly chosen due to their relatively close ionic radii to the ionic radius of Zn^{2+} ions and the ease of replacing Zn^{2+} ions without changing the ZnO crystalline structure over a wide range of dopant concentrations. Literature review had revealed the application of such metal dopants in photodegradation process. However, either small

molecules or lengthy synthesis procedure or expensive light sources or long treatment time was used [16–18].

The aim of the work was to conduct a comparative study on the effect of Mg, Cu and Sn doping on ZnO NPs. Doped ZnO NPs were synthesized via a simple, economic co-precipitation method. The synthesized NPs were then characterized and the effect of the metal dopants on the optical properties of ZnO NPs was compared. A visible LED photocatalytic protocol was established for treatment of pharmaceutical wastewater containing citalopram (CIT), as a model selective serotonin reuptake inhibitor antidepressant in wastewater (Fig. S1 of Supplementary Materials). The photocatalytic degradation of CIT was observed to study the influence of different metal doping on the performance of ZnO NPs. To the best of our knowledge, the use of metal doped ZnO NPs as a photocatalyst in photocatalytic degradation of CIT has not been reported yet. Optimization of the photocatalytic degradation process using the metal dopants was carried out through full factorial experimental design. The kinetics of CIT degradation was studied. Application of the optimized protocol to incurred wastewater samples, collected during the pharmaceutical cleaning process of CIT production lines was also investigated. The introduced approach can be performed as an economic and low cost route to facilitate the integration of the outstanding potential of visible LED photocatalysis in more industrial applications and waste water treatment.

2 Experimental

2.1 Chemicals and reagents

Anhydrous zinc acetate $(Zn(CH_3COO)_2)$ and magnesium chloride $(MgCl_2)$ were purchased from Sigma-Aldrich (USA). Stannous chloride dihydrate $(SnCl_2.2H_2O)$ as well as copper acetate monohydrate $(Cu(CH_3COO)_2.H_2O)$ were purchased from Loba Chemie (India). CIT standard (purity 98.89%) as well as incurred water samples were kindly supplied by Delta Pharmaceutical Industries (Egypt). 0.1 M Phosphate buffer (using monobasic potassium phosphate solution and then adjusting the pH using 0.2 M NaOH according to US Pharmacopoeia). 50 mM borate buffer (prepared by appropriate dilution of 0.5 M stock solution of sodium tetraborate decahydrate, adjusting the pH with 0.1 M NaOH and completing the volume to 25 mL with distilled water). Deionized water was used throughout the synthesis of NPs. All chemicals and solvents were of analytical grade.

2.2 Instruments

A commercially available 48 W LED lamp, kept in an air-ventilated chamber, was used for visible light irradiation.

Agilent capillary electrophoresis 7100 system, using Chemstation software was used (Agilent Technologies, Germany). The morphology of all NPs were characterized using a high resolution transmission electron microscope (HR-TEM) (TEM 2100; JEOL, Japan). X-ray diffraction (XRD) graph was recorded on a Bruker D8- Advance diffractometer (Bruker AXS, USA). NOVA touch 4LX analyzer (Quantachrome, USA) was used for Brunauer–Emmett–Teller (BET) measurements. UV-Vis diffuse reflectance spectra (DRS) of NPS were observed using Jasco V-770 spectrophotometer (Japan). Zeta potential was measured using Zetasizer Nano ZS-ZEN 3600 (Malvern Instruments, UK). Statistical analysis and experimental design were performed using Minitab, ver. 16.1.1 (Minitab, USA).

2.3 Synthesis and characterization of NPs
2.3.1 Synthesis of undoped ZnO NPs
A facile co-precipitation approach was used for the preparation of pure and doped ZnO NPs. In 100 mL deionized water, 0.1 M anhydrous $Zn(CH_3COO)_2$ (1.83 g) and 0.2 M NaOH (0.80 g) aqueous solutions were prepared separately, then mixed and magnetically stirred at 750 rpm for 2 h at 60 ℃ until a white precipitate was formed. The precipitate was separated from the solution by centrifugation at 4000 rpm for 10 min and then washed for three times with water and ethanol. Finally, the precipitate was dried at 60 ℃ for 2 h and then calcined at 600 ℃ for 6 h.

2.3.2 Synthesis of doped ZnO NPs
Doped ZnO NPs was prepared according to previously reported methods but with slight modifications of temperature and time [19–21]. (i) For Mg doped ZnO NPs (Mg/ZnO), $MgCl_2$ was used with three molar percentages relative to zinc 3, 5, and 7% mol (0.02 g, 0.04 and 0.06 g respectively). Different amounts of $MgCl_2$ were mixed with 100 mL 0.2 M (0.80 g) NaOH solution. The solution was added dropwise to 100 mL 0.1 M (1.83 g) anhydrous $Zn(CH_3COO)_2$ solution and stirred at 750 rpm for 2 h at 60 ℃. (ii) For Cu doped ZnO NPs (Cu/ZnO), $Cu(CH_3COO)_2.H_2O$ was used in three molar percentages (0.54, 1.08 and 2.15% mol) (0.02 g, 0.05 and 0.11 g respectively) in the doping procedure. Different amounts of $Cu(CH_3COO)_2.H_2O$ were added dropwise to 50 mL 0.5 M (5 g) solution of anhydrous $Zn(CH_3COO)_2$ followed by slow addition of 25 mL of 2 M (2 g) NaOH. The solution was magnetically stirred at 350 rpm for 2 h at 70 ℃. (iii) For Sn doped ZnO NPs (Sn/ZnO), $SnCl_2.2H_2O$ of three different molar ratios 0.05, 0.1 and 0.125 M (0.22 g, 0.45 and 0.56 g, respectively) prepared in 20 mL aqueous solution was added dropwise to 50 mL of 0.5 M (5 g) of anhydrous $Zn(CH_3COO)_2$. The solution was magnetically stirred for 30 min. Then, 50 mL of 2 M (4 g) NaOH

solution were added dropwise to the mixture. The solution was stirred magnetically at 500 rpm at 60 °C for 2 h until a white precipitate was formed. For all NPs, the precipitate was separated from the solution by centrifugation at 4000 rpm for 10 min and then washed three times with deionized water and ethanol. The precipitate was then dried at 60 ℃ for 2 h and calcined at 600 ℃ for 6 h and 4 h for Mg/ZnO and Cu/ZnO respectively. While, Sn/ZnO was calcined at 300 ℃ for 4 h.

2.3.3 Characterization of NPs
The synthesized undoped and doped ZnO NPs were inspected for their morphology and size distribution using HR-TEM. Few sample drops were put on a carbon coated copper grid, left to dry and then examined at 200 kV. XRD graph of NPs was recorded on a Bruker D8- Advance diffractometer with backgroundless sample holders and the X-ray generator was operated at 40 kV and 30 mA. Surface area measurements such as specific surface area ($m^2\ g^{-1}$), pore volume ($cm^3\ g^{-1}$), total pore volume ($cm^3\ g^{-1}$), average pore radius (nm) and nitrogen adsorption–desorption isotherms of the NPs were also estimated based on BET theory. Measurements of reflectance – absorbance in the UV–Vis range were used to calculate the optical parameters and to study the influence of metal dopant on the optical band gap of ZnO NPs. Barium sulphate powder was used as a standard for baseline measurements and the spectra were recorded in a range of 200–800 nm. Using Nano ZS-ZEN 3600 Zetasizer at 25 °C for 120 s, the average zeta potential of NPs was calculated. Zeta potential measurements were carried out to evaluate the colloidal stability of NPs at different pH of 5, 7 and 9.

2.4 Development of capillary zone electrophoresis (CZE) separation
Bare fused silica capillaries (Agilent Technologies, Germany) 50-µm (id), 325-µm (od) with a total/effective length of 33.0/24.5 cm were used in all investigations. Before each run, preconditioning of the capillary was done according to the manufacturer's specifications and previously optimized protocols. Capillaries were flushed using 0.1 M NaOH, Milli-Q water and finally with background electrolyte (BGE) for 5 min each. The effect of pH and composition of the BGE were investigated. Samples were injected hydrodynamically at 5 kPa for 5 s and 50 mM borate buffer at pH 10 was used as the BGE. Separation was carried out at 25 °C using an applied voltage of 13 kV (positive polarity) and detection wavelength of 200 nm. Calibration curve for CIT was constructed using standard series covering a concentration range of (1–50 µg mL^{-1}). Regression equation was obtained and used for calculation of residual CIT concentration

throughout the study. Separation efficiency was demonstrated using CIT degraded sample. Validation was done according to ICH Guidelines: Topic Q2 (R1) Validation of Analytical Procedures. Validation parameters were determined: accuracy, precision, linearity and limit of detection. System suitability parameters were then calculated according to US Pharmacopoeia.

2.5 Photocatalytic degradation study

2.5.1 Preliminary studies

First, 50 µg mL^{-1} standard CIT samples were prepared in phosphate buffer pH 5, 7 and 9 and were left in dark at room temperature for 2 h. Then, two CIT samples (50 µg mL^{-1}) were prepared in phosphate buffer pH 7 and exposed to LED irradiation for 2 h in the absence and presence of pure ZnO NPs (0.5 mg mL^{-1}). For comparative purposes, same experimental conditions were

applied for nine CIT samples using (i) (3, 5, and 7% mol) Mg/ZnO (ii) (0.54, 1.08 and 2.15% mol) Cu/ZnO and (iii) (0.05, 0.1 and 0.125 M) Sn/ZnO to investigate the effect of different dopant ratios on CIT photodegradation. Finally, all samples were analyzed using the CZE assay.

2.5.2 Experimental design

The effects of dopant, initial CIT concentration, catalyst loading, and pH were studied. Two levels were arbitrarily assigned for each of the four factors (2^4) either low (-1) or high (+1) as shown in Table 1. Sixteen sets of experimental conditions (two-level full factorial design 2^4) were done as illustrated in Table 2. All experiments were performed at room temperature, in an air ventilated chamber while magnetically stirred. Before exposure to LED lamp, CIT and NPs mixture were stirred in dark for 30 min in order to achieve adsorption equilibrium. All through the study, visible light radiation of 25 mL of buffered CIT solution and NPs was carried out as shown in each experiment in Table 2. At the end of the incubation period, samples were completed to volume (25 mL), filtered through a syringe filter (0.2 µm) and then analyzed using the CZE assay as previously described.

2.6 Kinetics of CIT photocatalytic degradation

Kinetics of CIT photocatalytic degradation reaction was studied using both Sn/ZnO and Cu/ZnO over 2 h at 20 min intervals. Photocatalytic degradation was performed at the optimum set of conditions: CIT (25 µg

Table 1 Actual factors and the levels used in two-level full factorial design experiment

Factor Name	Factor code	Low level (-1)	High level (+1)
Dopant	A	Cu	Sn
Catalyst loading (mg mL^{-1})	B	0.5	1
pH	C	7	9
Initial CIT concentration (µg mL^{-1})	D	25	50

Table 2 Design matrix for 2^4 full factorial experimental design constructed for photocatalytic degradation of CIT and results obtained through CZE assay

Run no.	Factor code				CZE	
	A	B	C	D	CIT concentration (µg mL^{-1})	% Photodegradation
1	Sn	-1	-1	-1	5	80
2	Sn	+1	-1	+1	24	51
3	Cu	+1	+1	+1	21	58
4	Sn	-1	+1	-1	11	58
5	Cu	+1	+1	-1	9	65
6	Cu	-1	-1	+1	20	61
7	Sn	+1	+1	-1	11	56
8	Cu	-1	-1	-1	10	60
9	Sn	-1	+1	+1	23	53
10	Cu	+1	-1	+1	26	48
11	Sn	+1	-1	-1	8	68
12	Cu	+1	-1	-1	12	53
13	Cu	-1	+1	+1	19	63
14	Sn	+1	+1	+1	20	59
15	Cu	-1	+1	-1	8	68
16	Sn	-1	-1	+1	15	71

Nazim *et al. Sustainable Environment Research*   (2023) 33:39

Page 6 of 16

mL^{-1}, pH 7) in the presence of Sn/ZnO (0.5 mg mL^{-1}) and CIT (25 μg mL^{-1}, pH 9) in the presence of Cu/ZnO (0.5 mg mL^{-1}). CZE assay was employed to monitor CIT concentration gradual decrease over time.

2.7 Application to incurred samples
Two cycles of cleaning validation of CIT production lines were performed according to the manufacturer's protocols. Briefly, a commercially available alkaline wash solution (Alcojet $^{®}$) was used in the first cycle, followed by purified water in the second one. Samples were collected during each washing cycle and stored at -20 °C. Prior to analysis, pH was adjusted to 7 and 9 and CIT concentration was then determined. Subsequently, the samples (25 mL) were subjected to LED lamp in the presence of both Sn/ZnO and Cu/ZnO (0.5 mg mL^{-1}) for 2 h. After the irradiation period, CIT concentration and the percentage of degradation were determined.

3 Results and discussion
3.1 Synthesis of undoped and doped ZnO NPs
Pure ZnO, Mg, Cu and Sn doped ZnO NPs were synthesized via simple co-precipitation method using no hazardous chemicals. Among various methods, co-precipitation is such a facile cost effective technique with short synthesis time, low reaction temperature, small particle size, high porosity and purity, strong chemical homogeneity and crystallinity [22]. To study the effect of molar ratio of metal doping on ZnO, each of Mg, Cu and Sn were used, in three different ratios during the preparation of NPs. All NPs were implemented in visible light-driven photocatalytic degradation of CIT for screening

purposes. The ratio of each metal that resulted in high percent degradation was used for further comparative studies.

3.2 Characterization of NPs
3.2.1 XRD
The crystalline structure of the synthesized undoped and doped ZnO NPs was analyzed by XRD (Fig. 1a). Data showed sharp diffraction peaks at 2θ and the corresponding plane coordinates were 31.4° (100), 34.0° (002), 36.8° (101), 47.0° (102), 56.1° (110), 63.4° (103), 67.5° (200) and 68.6° (112). Three characteristic ZnO diffraction peaks (100), (002) and (101) appeared at 2θ = 31.4°, 34.0° and 36.8°. The diffraction patterns can be indexed to wurtzite hexagonal phase of ZnO (JCPDS No: 36–1451). XRD patterns of undoped and doped ZnO NPs showed similar diffraction peak positions. There were no other diffraction peaks related to the dopant. This is due to the substitution of Zn^{+2} ions with Mg^{+2}, Cu^{+2} and Sn^{+4} ions because of their relatively close ionic radii. So, there was no considerable impact on the crystalline structure of ZnO and also did not obviously shift the diffraction peaks as shown in (Fig. 1b). No peaks were observed as secondary phases of impurities, indicating high purity of the ZnO NPs. Moreover, all peaks were sharp and intense, which indicated that samples were highly crystalline. The average crystallite size was estimated using the Debye-Scherrer's equation by measuring the full width at half maximum of the most intense diffraction peak [23]. D = 0.9λ/βcosθ, where d is the average crystallite size, λ is the wavelength, β is the angular width of the diffraction peak at the half maximum (FWHM) on the 2θ scale, θ is
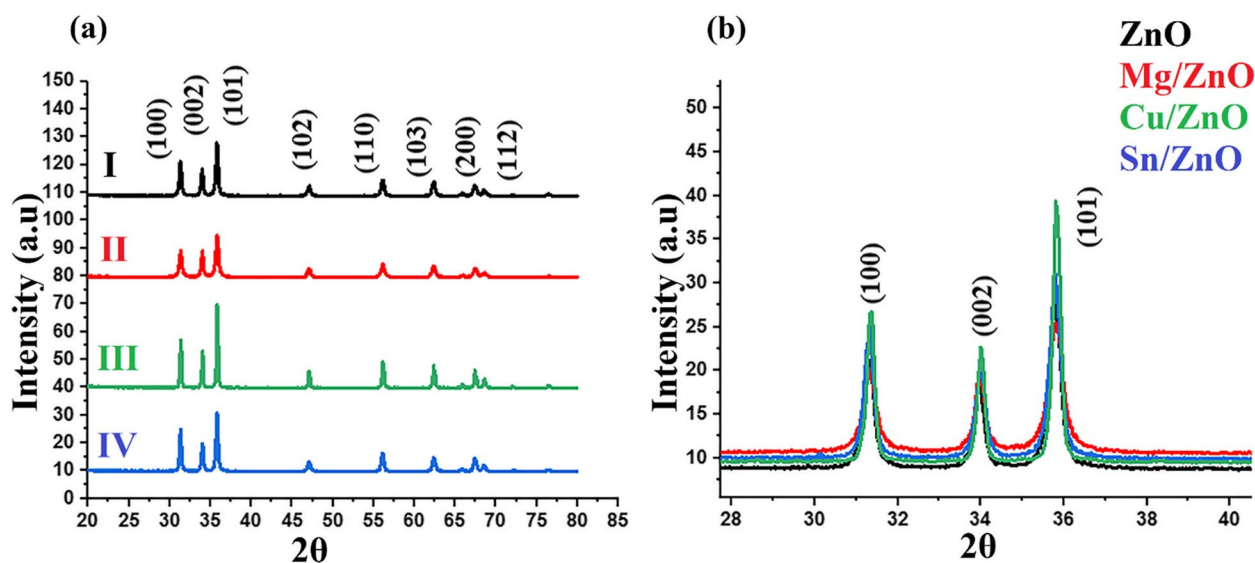

Fig. 1 **a** XRD patterns of (I) undoped ZnO (II) Mg/ZnO (III) Cu/ZnO (IV) Sn/ZnO. **b** High-resolution XRD patterns of undoped and doped ZnO NPs

the angle of diffraction. The calculated values of average crystallite size were 57, 41, 35 and 31 nm for ZnO NPs, Mg/ZnO, Cu/ZnO and Sn/ZnO, respectively. It can be noticed that the average crystallite size of doped ZnO is smaller than that of undoped ZnO. This comes in agreement with previous literature [24, 25] that the decrease in the crystallite size upon the doping of ZnO may be due to the formation of deformed lattice structure and more defects which could be due to strain induced by ions' substitution.

3.2.2 TEM
The morphology and size distribution of NPs was investigated using HR-TEM (Fig. 2). Results showed the formation of spherical NPS with a mean hydrodynamic diameter of 56, 38, 50 and 28 nm for ZnO NPs, Mg/ZnO, Cu/ZnO and Sn/ZnO, respectively. The size obtained through TEM analysis was in accordance with the size obtained through XRD data. Although the NPs size decreased with metal dopants the shape of the NPs remained spherical type as shown in Fig. 2.

3.2.3 BET
BET analysis was used to estimate the specific surface area of NPs while the pore size and pore volume of NPs were estimated by the Barrett-Joyner-Halenda model from the adsorption-desorption isotherm, as shown in Table S1. The specific surface area of doped ZnO was found to be higher than pure ZnO NPs. As acknowledged by XRD analysis, with the doped ZnO, the crystallite size decreases; consequently, surface area increases. Sn/ZnO was found to have the highest specific surface area (37 m^2 g^{-1}). The high surface area of NPs obtained had allowed better contact for CIT and thus high photocatalytic properties. Nitrogen adsorption–desorption isotherm showed type IV isotherm with H3 hysteresis loop of which is characteristic for mesoporous materials (Fig. 3). The pore radius of all the NPs was found to be 1.91–1.93 nm revealing mesoporous nature of these materials.

3.2.4 DRS
The DRS spectra of undoped and doped ZnO NPs are shown in Fig. 4a in the wavelength range of 200–800 nm. The ZnO absorption edge was about 350 nm, indicating no absorption in the visible range. However, after doping with Mg, Cu and Sn, its absorption edge is shifted to the visible range. The optical band gap of the NPs was evaluated from diffuse reflectance spectra by plotting square of the Kubelka–Munk function against excitation energy (Eg) [26]. The band gap energy of ZnO NPs was found to be 3.34 eV whereas the band gap energy was 3.21, 3.15 and 3.05 eV for Mg/ZnO, Cu/ZnO and Sn/ZnO
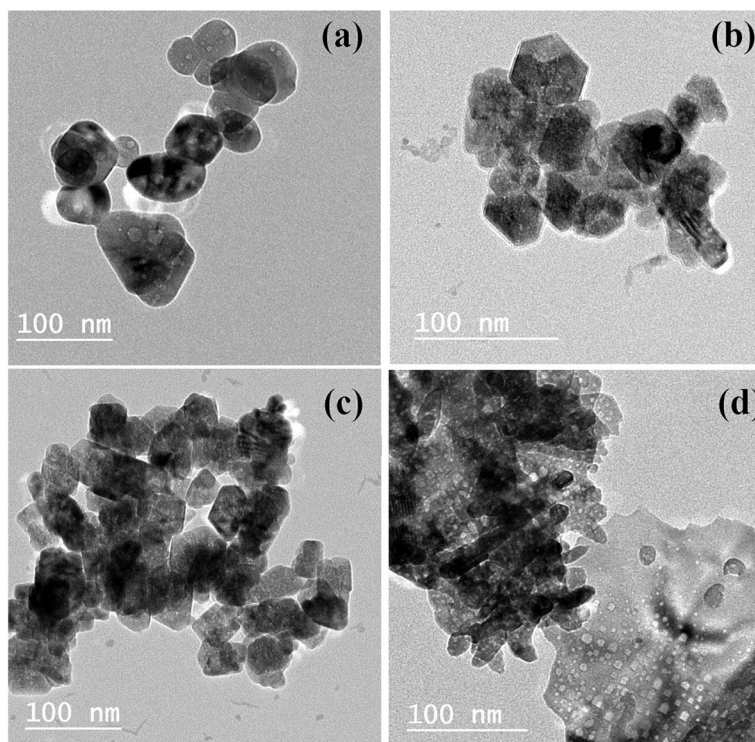

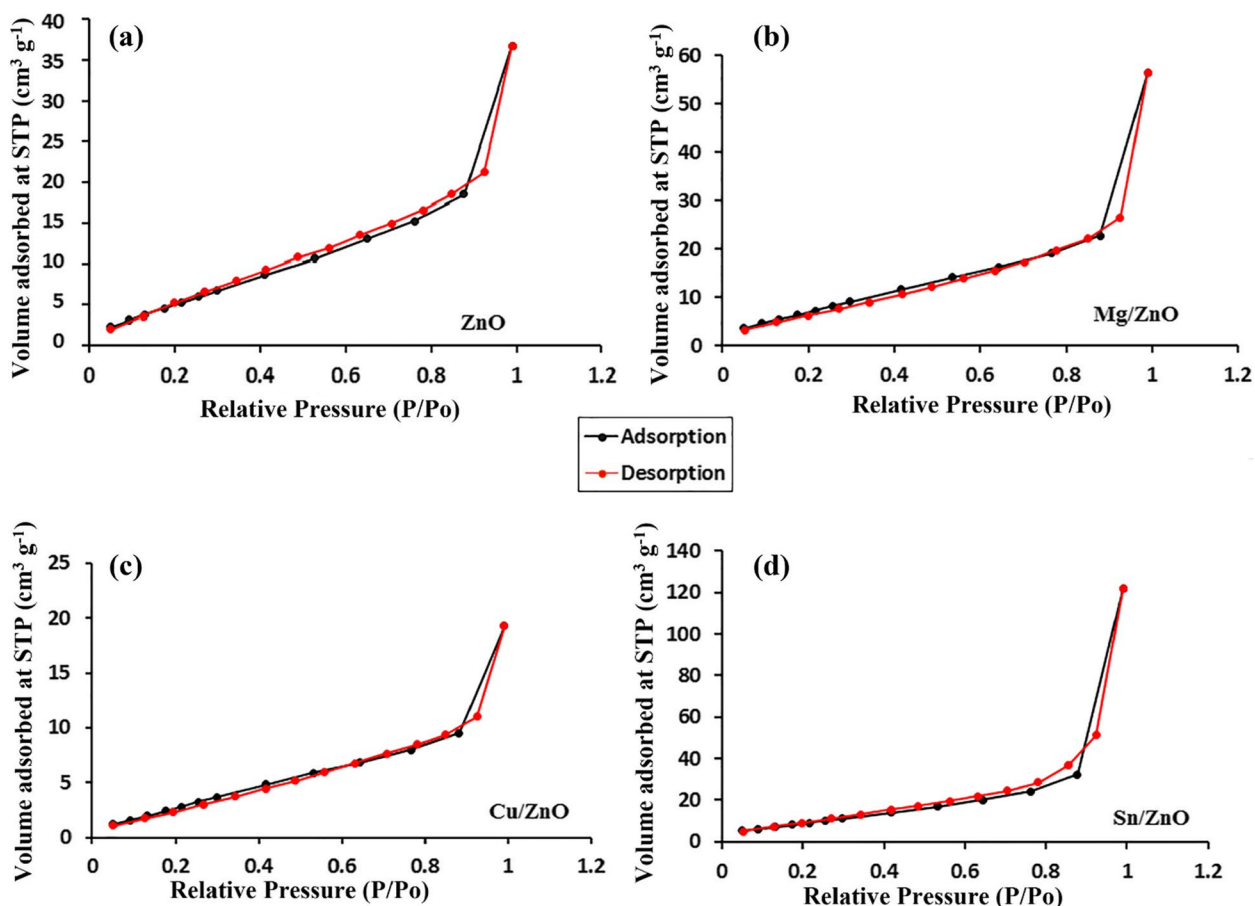**Fig. 2** Transmission electron micrograph of (**a**) undoped ZnO (**b**) Mg/ZnO (**c**) Cu/ZnO (**d**) Sn/ZnO

Fig. 3 Nitrogen adsorption–desorption isotherms (**a**) undoped ZnO (**b**) Mg/ZnO (**c**) Cu/ZnO (**d**) Sn/ZnO
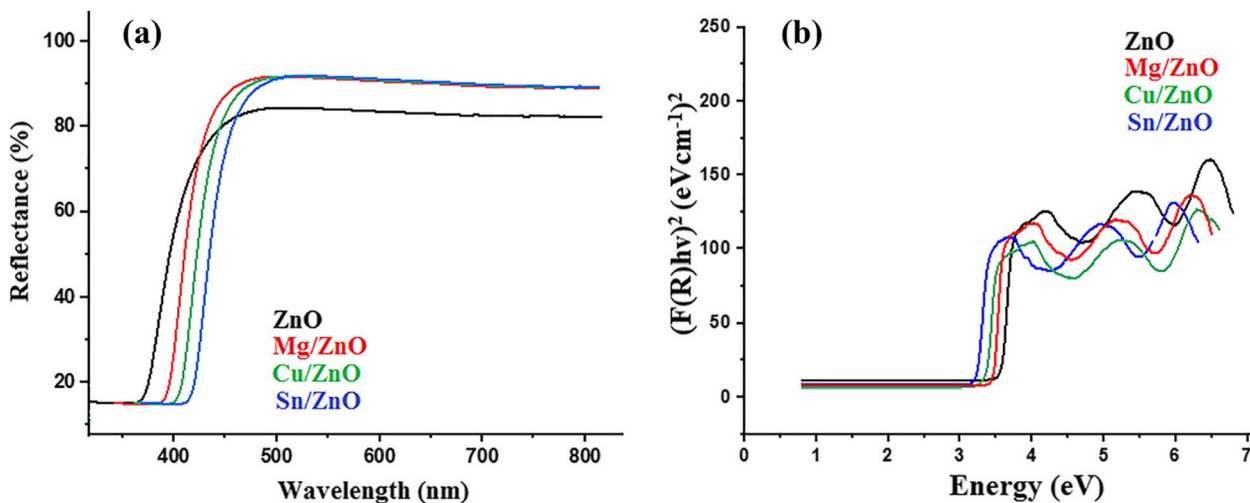

Fig. 4 a UV-Vis diffuse reflectance spectra of undoped and doped ZnO NPs. **b** Band gap energy (Eg) of undoped and doped ZnO NPs

respectively (Fig. 4b). Results showed that the band gap energy decreased after doping ZnO NPs with different metals, consequently improving the photocatalytic activity of the photocatalysts under visible light.

3.3 Development of CZE

A CIT photodegraded sample was prepared (as mentioned previously) and used during development and optimization of the CZE assay. The effect of BGE

composition on the electrophoretic separation was studied. Borate buffer showed better resolution than phosphate buffer. The effect of pH was also studied and pH 10 was found to enhance sharpness and peak symmetry when compared to pH 8 and 9. Good resolution was obtained over 5 min using the assay conditions as described above. An equivalent CIT sample was prepared and had not been subjected to LED irradiation as a control sample to verify the identity of CIT and calculate the percentage of photodegradation as well. System suitability parameters (according to US Pharmacopoeia) and also validation parameters (according to ICH guidelines) were calculated and summarized in Table 3.

3.4 Photocatalytic degradation study

3.4.1 Preliminary studies

CIT is a commonly prescribed antidepressant drug that was detected in different water sources [27]. Initially, CIT hydrolytic stability was confirmed at pH 5, 7 and 9 at room temperature over 2 h (data not shown). Results were in agreement to the previously reported data showing the relative stability of CIT [28]. Then, CIT

Table 3 Summary of system suitability and validation parameters for the developed CZE assay

System suitability parameters	
Retention time (min)	2.9
Asymmetric factor (T)	0.8
Selectivity (α)	1.2
Resolution (Rs)	4.3
Number of theoretical plates (N)	20,927
Validation parameters	
Accuracy (mean ± SD)[a]	100.7 ± 1.0
Precision (%RSD)	
Repeatability [b]	0.5
Intermediate precision [c]	1.6
Linearity	
Regression equation	Y = 1.79 + 6.81
Correlation coefficient (r)	0.9997
Range (μg mL^{-1})	1–50
LOD (μg mL^{-1}) [d]	0.2
LOQ (μg mL^{-1}) [e]	0.3
Robustness (mean ± SD) [f]	0.8 ± 0.01

[a] Average percentage recovery of nine determinations over three concentration levels

[b] The intraday, average of nine determinations over three concentration levels repeated three times within the same day

[c] The interday, average of nine determinations over three concentration levels repeated three times over three different days

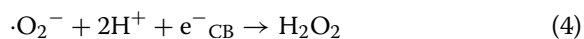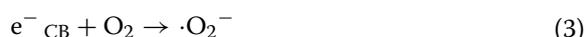[d] LOD determined via calculations, 3.3 (SD of the response/slope)

[e] LOQ determined via calculations, 10 (SD of the response/slope)

[f] Asymmetric factor: Average of nine determinations over three concentration levels

samples (50 μg mL^{-1}) were subjected to LED irradiation at pH 7 for 2 h in the absence and presence of ZnO NPs. In the presence of visible light only, 15% degradation was obtained while the addition of pure ZnO NPs resulted in 28% degradation (Fig. S2 of Supplementary Materials).

Preliminary screening of the effect of Mg, Cu and Sn dopant ratios on CIT visible light-driven photocatalysis was carried out (CIT 50 μg mL^{-1}, pH 7, 0.5 mg mL^{-1} NPs). A percentage degradation of 51, 62 and 71% were obtained in case of Mg, Cu and Sn doping, respectively (Table 4). 7% mol Mg/ZnO, 1.08% mol Cu/ZnO and 0.1 M Sn/ZnO had resulted in higher CIT percent degradation relative to other dopant ratios (Table 4). Sn/ZnO showed the highest percent degradation followed by Cu/ZnO and then Mg/ZnO. Doping decreased the band gap energy of ZnO NPs as previously mentioned. This indicated that less energy would be required to excite an electron from the valence band into the conduction band and the wavelength required to be absorbed would be shifted towards the visible range and improve photocatalytic activity.

When ZnO is photo-induced by visible light with photonic energy (hv) equal to or greater than the Eg, electrons from the filled valence band (VB) are promoted to an empty conduction band (CB). This photo-induced process produces electron-hole (e$^-$/h$^+$) pairs (step 1). The e$^-$/h$^+$ pairs migrate to ZnO surface and are involved in redox reactions. The H$^+$ reacts with water and hydroxide ions to produce hydroxyl radicals (step 2) while e$-$ reacts with oxygen to produce superoxide radical anions then hydrogen peroxide (step 3 and 4). Hydrogen peroxide will then react with superoxide radicals to form hydroxyl radicals (step 5). The resulting hydroxyl radicals, which are powerful oxidizing agents, will attack CIT on the surface of ZnO to rapidly produce intermediate degradation compounds (step 6) [29]. The major constraint of ZnO as

Table 4 Visible light-driven CIT photocatalysis using Mg, Cu and Sn doped ZnO NPs and different dopant ratios (CIT 50.00 μg mL^{-1} at pH 7.0 in the presence of 0.5 mg mL^{-1} NPs)

Dopant	Dopant ratio	% photodegradation
Mg doped ZnO	3% mol	44
	5% mol	47
	7% mol	51
Cu doped ZnO	0.54% mol	59
	1.08% mol	61
	2.15% mol	54
Sn doped ZnO	0.05 M	61
	0.1 M	72
	0.125 M	53

a photocatalyst is the rapid recombination rate of photogenerated e^-/h^+ pairs, which decreases the photodegradation reaction. Doping has thus been used to modify the physical and chemical properties of ZnO by incorporating metals to shift narrow the bandgap energy to the UV-Vis region.

$$Doped\ SnO\ +\ visible\ light \rightarrow h_{VB}^+ + e^-_{CB} \quad (1)$$

$$H_2O\ +\ h_{VB}+ \rightarrow\ \cdot OH\ +\ H^+ \quad (2)$$

$$e^-_{CB} + O_2 \rightarrow \cdot O_2^- \quad (3)$$

$$\cdot O_2^- + 2H^+ + e^-_{CB} \rightarrow H_2O_2 \quad (4)$$

$$H_2O_2 + \cdot O_2^- \rightarrow \cdot OH + H^+ \quad (5)$$

$$\cdot OH\ +\ CIT \rightarrow Photodegradation\ byproducts \quad (6)$$
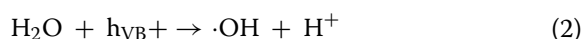
In addition, doping also can contribute to a greater production of •OH radicals, thus, lead to a higher degradation efficiency. By varying dopant ratio, the band gap can be tuned which affects the photocatalytic efficiency. Owing to their relatively high activity, Sn and Cu dopants only (0.1 M Sn/ZnO and 1.08% mol Cu/ZnO) were used to investigate the optimal experimental conditions for each. Preliminary screening of the effect of pH was carried out in the presence of Sn/ZnO and Cu/ZnO (CIT 50 μg mL^{-1} – 0.5 mg mL^{-1} NPs). A relatively low degradation was obtained at pH 5 (62 and 54% for Sn/ZnO and Cu/ZnO NPs, respectively). While the percent degradation had increased to 71% at pH 7 for Sn/ZnO NPs and 63% at pH 9 for Cu/ZnO NPs (Fig. 5). Results showed that the maximum degradation was obtained at pH values of 7 and 9, where the available hydroxyl ions can react with holes (h^+) to form hydroxyl radicals, which have high oxidation capability, and thus enhancing the photodegradation efficiency. At low pH values (pH 5), the photodegradation decreased due to high concentration of protons, which had high affinity for the hydroxyl anion, preventing the formation of hydroxyl radicals. These results were supported by zeta potential measurement to investigate the surface charge and the colloidal stability of NPs. Measurements were carried out

in phosphate buffer pH 5, 7 and 9. Optimum potential was achieved at pH 7 for Sn/ZnO NPs (-44 mv) and at pH 9.0 for Cu/ZnO NPs (-41 mv) which was sufficient to avoid aggregation and to form an intra molecular repulsive barrier. While pH 5 showed the least colloidal stability with zeta potential of -25 and −26 mv for Sn/ZnO and Cu/ZnO respectively. Therefore, pH 7 and 9 were further studied for both Sn/ZnO and Cu/ZnO. It should be noted that decreasing the irradiation time for 1 h had reduced the catalytic activity to 46 and 39% for Sn and Cu, respectively. Thus, a 2 h treatment protocol was used for further optimization.

3.4.2 Experimental design

Further investigation was conducted using Sn/ZnO and Cu/ZnO in order to optimize the effects of (A) dopant, (B) catalyst loading, (C) pH and (D) initial CIT concentration on the photodegradation efficiency. High concentration of CIT (up to 50 μg mL^{-1}) was used to cover the expected range in pharmaceutical wastewater. 0.5 mg mL^{-1} NPs loading was chosen as a common starting point in different photocatalytic procedures [30]. Full factorial design was used to assess the relative significance of the mentioned factors, their interactions as well as the optimal set of experimental conditions for CIT photocatalytic degradation (Table 1). Samples were then analyzed in duplicate using the developed CZE assay with the percentage degradation shown in Table 2.

Analysis of full factorial design results was done at 95% confidence level (P 0.05) using the percentage of degradation as the response factor. The relative magnitude of the studied factors and their interactions was visualized using pareto diagram. The direction of effects was illustrated by the normal plot of the standardized effects (Fig. 6). In this study, initial CIT concentration (D) was found to have significant impact with a negative effect indicating an increase in photocatalysis at low levels. Also, the interaction between the dopant (A) and pH (C) has significant impact. A 22% increase in Sn/ZnO photocatalytic activity was obtained upon decreasing the pH from 9 to 7. While Cu/ZnO showed 8% increase in the photodegradation at pH 9. This could be attributed to the NPs colloidal stability as mentioned before and CIT positive ionization at pH 7 (pKa 9.78). In addition, increasing the NPs loading to 1 mg mL^{-1} was found to be non-significant. This could suggest a plateau effect for the catalyst over a range of 0.5–1 mg mL^{-1}.

Maximum photodegradation (80%) was obtained at pH 7 in the presence of 25 μg mL^{-1} CIT and 0.5 mg mL^{-1} Sn/ZnO in 2 h. Whereas, 68% degradation was obtained at pH 9 in the presence of 25 μg mL^{-1} CIT and 0.5 mg mL^{-1}
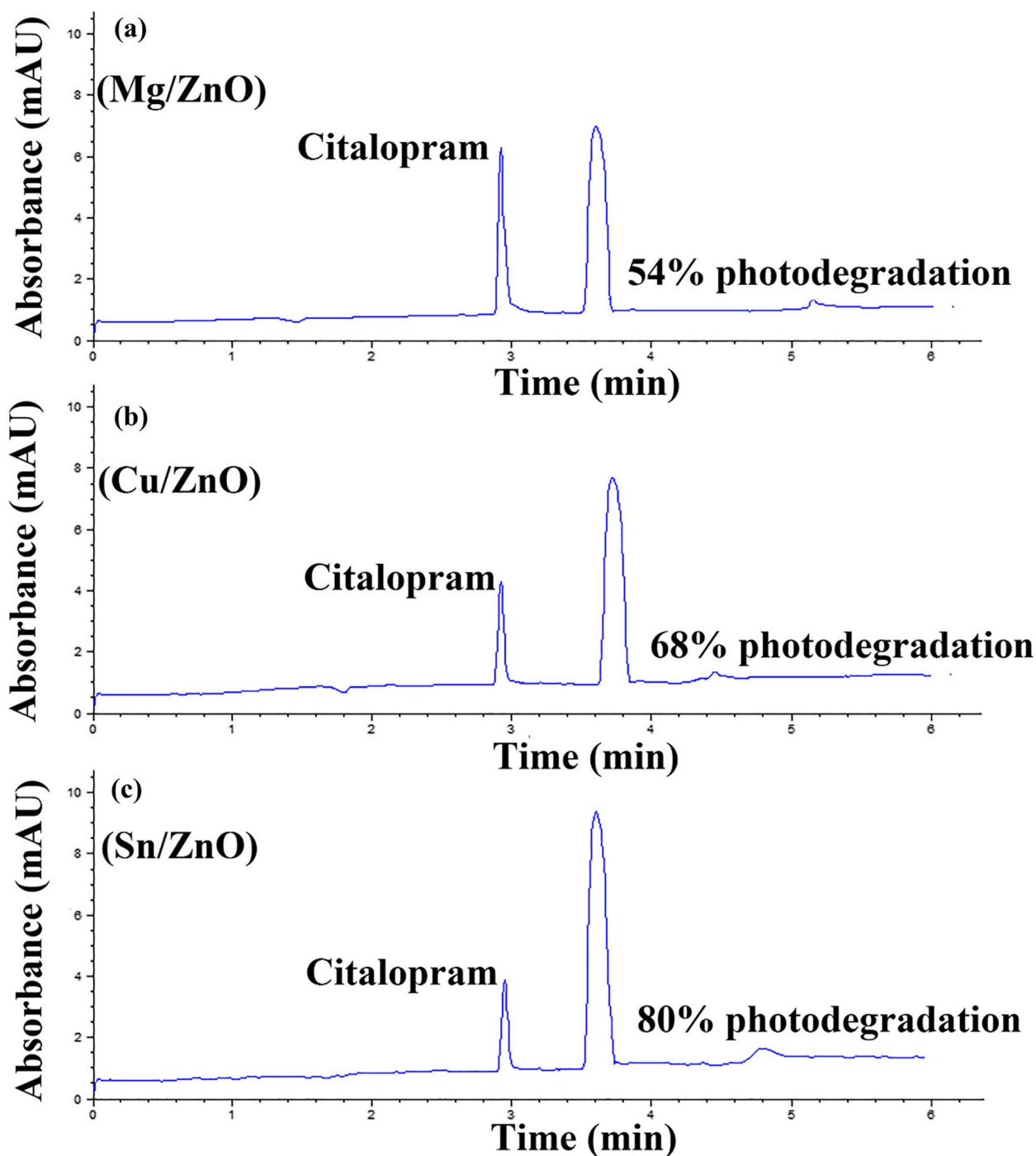
Fig. 5 CZE electropherogram of CIT (25 μg mL^{-1}) photocatalytic degradation upon exposure to 48 W LED lamp for 2 h at (**A**) pH 7 in the presence of 0.5 mg mL^{-1} Mg/ZnO. **B** pH 9 in the presence of 0.5 mg mL^{-1} Cu/ZnO. **C** pH 7 in the presence of 0.5 mg mL^{-1} Sn/ZnO

Cu/ZnO in 2 h. Both treatment protocols were chosen as optimum set for Sn and Cu dopants and were used for further investigation**s** (Table 2).

The regression equation summarizing the experimental design is given as follows:

$$\begin{aligned} Y =\ & 181.86 + 88.17A - 80.05B - 11.70C - 2.42D \\ & + 4.02AB - 10.40AC - 0.80AD + 7.36BC + 0.75BD \\ & + 0.22CD - 0.87ABC - 0.94ABD + 0.09ACD - 0.04BCD \end{aligned}$$

where Y = % degradation, A = dopant, B = dopant loading, C = pH and D = initial CIT concentration.
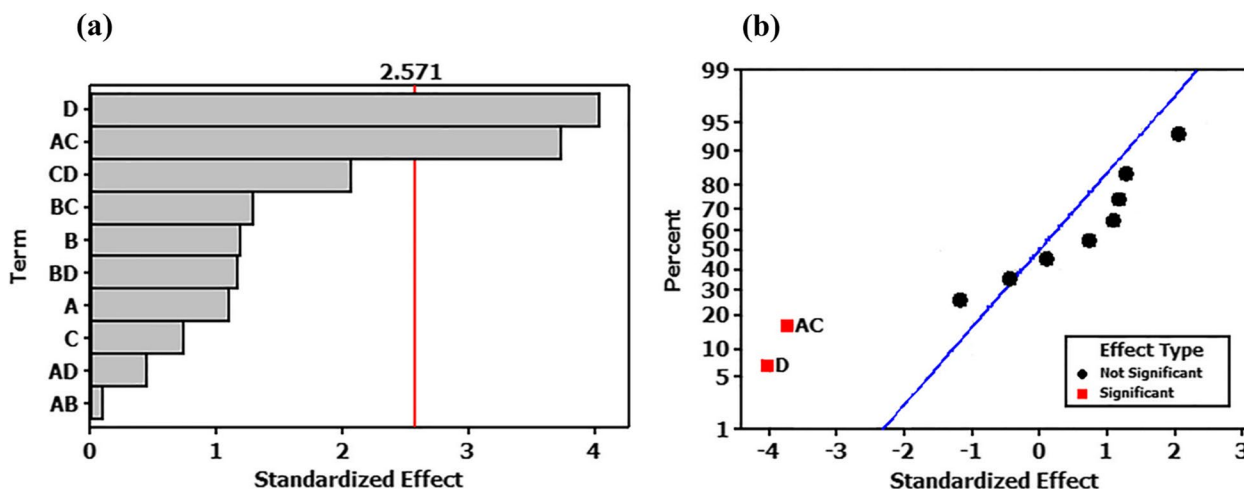
Fig. 6 a Pareto chart of the standardized effects of single and interaction factors on CIT photodegradation. **b** Normal plot of the standardized effects of single and interaction factors on CIT photodegradation

ANOVA was carried out and the results were calculated as shown in Table 5. A lack of fit value of 0.422 was observed indicating its non-significance and an acceptable predictability of the studied model. It should be noted that the efficacy of pure ZnO upon UV irradiation was studied by our group and only 45% CIT photodegradation was obtained. In addition, the photodegaradation of CIT had been previously reported. Although relatively high degradation was obtained, either UV light sources [31] or gamma radiation [32] or expensive NPs have been used. Thus, the synthesized doped ZnO NPs could spare the need of high energy UV lamps. Moreover, the studied treatment used economic household LED light, minimizing energy cost for large scale wastewater treatment process without comprising the degradation efficiency. Literature review had revealed the application of Mg [16], Cu [20] or Sn [17] doping for ZnO photocatalysis with acceptable degradation efficiency. However, either small molecules/dyes or lengthy synthesis procedure [16] or expensive high energy visible light sources [17] or long

Table 5 Analysis of variance for CIT photocatalytic degradation

Source of variation	Degree of freedom	Sum of squares	Mean of squares	*F* value	*P* value*
Main effects	4	420.0	105.0	5.6	0.3
A	1	46.4	46.4	2.5	0.4
B	1	29.0	29.0	1.5	0.4
C	1	10.9	10.9	0.6	0.6
D	1	333.7	333.7	17.7	0.2
2 way interactions	6	439.1	73.2	3.9	0.4
AB	1	0.2	0.2	0.01	0.9
AC	1	286.2	286.2	15.2	0.2
AD	1	3.9	3.9	0.2	0.7
BC	1	33.7	33.7	1.8	0.4
BD	1	27.8	27.8	1.5	0.4
CD	1	87.3	87.3	4.6	0.3
3 way interactions	4	99.9	25.0	1.3	0.6
ABC	1	15.5	15.5	0.8	0.5
ABD	1	1.2	1.2	0.07	0.8
ACD	1	82.9	82.9	4.4	0.3
BCD	1	0.3	0.3	0.01	0.9

*P value < 0.05 statistically significant difference

treatment time was used [18]. The photocatalytic performance of the synthesized doped ZnO NPS were compared to the recently reported studies (Table 6). It can be seen that our results established a relatively high photo-degradation efficiency with respect to the high molecular weight organic compound used (CIT), reaction time and the cost effective light source used.

3.5 Kinetics of CIT photocatalytic degradation

The kinetics of CIT photocatalytic degradation was studied using both Sn/ZnO and Cu/ZnO at optimum set of experimental conditions. CIT (25 µg mL^{-1}, pH 7) in the presence of Sn/ZnO (0.5 mg mL^{-1}) whereas CIT (25 µg mL^{-1}, pH 9) in the presence of Cu/ZnO (0.5 mg mL^{-1}). The kinetics was described using the Langmuir-Hinshelwood model [39] to accommodate reactions taking place at solid-liquid interface. $k_{obs}.t = \ln (Ct/Co)$ where Ct (µg mL^{-1}) is the concentration at any time t during the reaction and Co (µg mL^{-1}) is the initial concentration and k_{obs} (min^{-1}) is apparent rate constant. Upon plotting ln (Ct/Co) against time, a straight line was obtained which indicated a pseudo-first order kinetics (Fig. 7). From this figure, good linearity (r > 0.99) for both catalysts was obtained which showed the applicability of the Langmuir- Hinshelwood model for the photocatalytic degradation of CIT. The apparent rate constant k_{obs} and half-life $t_{0.5}$ values for the photocatalytic degradation reaction Half−life: $t_{0.5} = 0.693/ k_{obs}$ were calculated. The k_{obs} was 0.01 min^{-1} and $t_{0.5}$ of 64 min for Sn/ZnO while k_{obs} 0.0076 min^{-1} and $t_{0.5}$ of 92 min, upon using Cu/ZnO. The rate constant value of Sn/ZnO was approximately two times higher than that of Cu/ZnO resulting in better photocatalytic efficiency. The high photo degradation

efficiency of Sn/ZnO more than Cu/ZnO could be attributed to the difference in band potential. Sn/ZnO has band gap energy 3.05 eV while Cu/ZnO has band gap energy 3.15 eV. The smaller band gap energy of Sn/ZnO promotes the separation of the photogenerated electrons and holes faster than Cu/ZnO, and thus, decreases the e$^-$/h$^+$ pair recombination rate. The rate of degradation is related to the available catalyst surface for the generation of e$^-$/h$^+$ pair, which in turn generates free radicals. In this case, the amount of photocatalyst is kept constant and thus number of free radicals generated remains the same, while CIT concentration decreases by time.

3.6 Reusability of SnO$_2$/GA NPs

The capability to regenerate both Sn/ZnO and Cu/ZnO was investigated. 0.5 mg mL^{-1} of both NPs was added to two standard CIT buffered solutions (25 µg mL^{-1}) and subjected to LED lamp for 2 h. Then, both samples were centrifuged, washed well with deionized water, and left to dry in air for subsequent use. The recovered NPs were then reused in a second and third cycles for photocatalytic degradation of CIT under the same experimental conditions. Minimum decrease (ꞏ7%) in the photocatalytic activity was observed after three cycles (Fig. 8). The decrease in the NPS degradation efficiency might be attributed to deactivation of some active sites in the previous degradation cycle with the occurrence of minor photocorrosion process. Besides, the slight loss of photocatalyst during the catalyst recovery steps where constant stirring was used as well as washing after each run. Therefore, the reusability of both Sn/ZnO and Cu/ZnO did not significantly affect the photocatalytic owing to its

Table 6 Summary of recently reported methods of doped ZnO NPs photocatalysis

| Doped ZnO NPs	Studied model	Degradation efficiency	Comment	Ref
Sn/ZnO NPs Cu/ZnO NPs	Citalopram	- 78% in 120 min - 68% in 120 min	- Facile synthesis - Economic household LED lamp was used - High molecular weight organic compund	Current work
Sn doped ZnO NPs	Methylene blue	94% in 180 min	- Low molecular weight compound - Long treatment time	[18]
Cu doped ZnO NPs	Methylene green	75% in 240 min	- Simple dye - Long treatment time	[33]
Ag doped ZnO thin films	Methylene blue	45% in 140 min	- High cost of Ag used - Lengthy synthesis procedure	[34]
La doped ZnO	Methyl orange	85% in 150 min	- High cost of rare earth metal - Lengthy synthesis procedure	[35]
Ba doped ZnO NPs	Rhodamine B	98% in 68 min	- High watt visible light source (500 W) - Simple dye	[36]
Cu doped ZnO	Monocrotophos pesticide	80% in 180 min	- Lenghty synthesis procedure - Long treatment time	[37]
N-doped ZnO/graphene oxide	Brilliant smart green dye	Full degradation in 90 min	- High watt visible light source (300 W Xe lamp) - Lenghty synthesis procedure	[38]
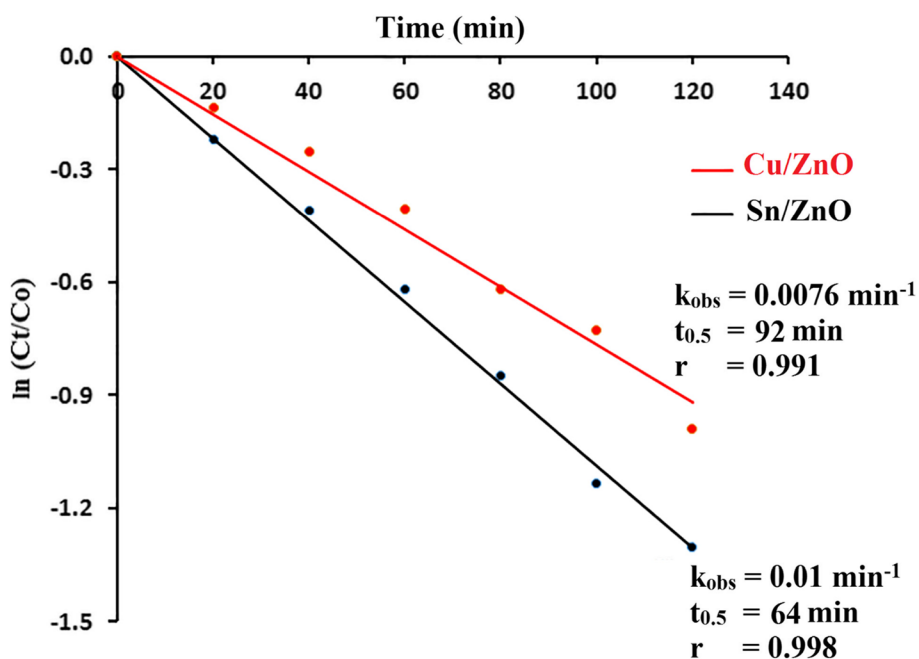
Fig. 7 Kinetics profile of CIT photodegradation with initial CIT concentration 25 µg mL^{-1} at pH 7 with 0.5 mg mL^{-1} Sn/ZnO and pH 9 with 0.5 mg mL^{-1} Cu/ZnO upon exposure to 48 W LED lamp
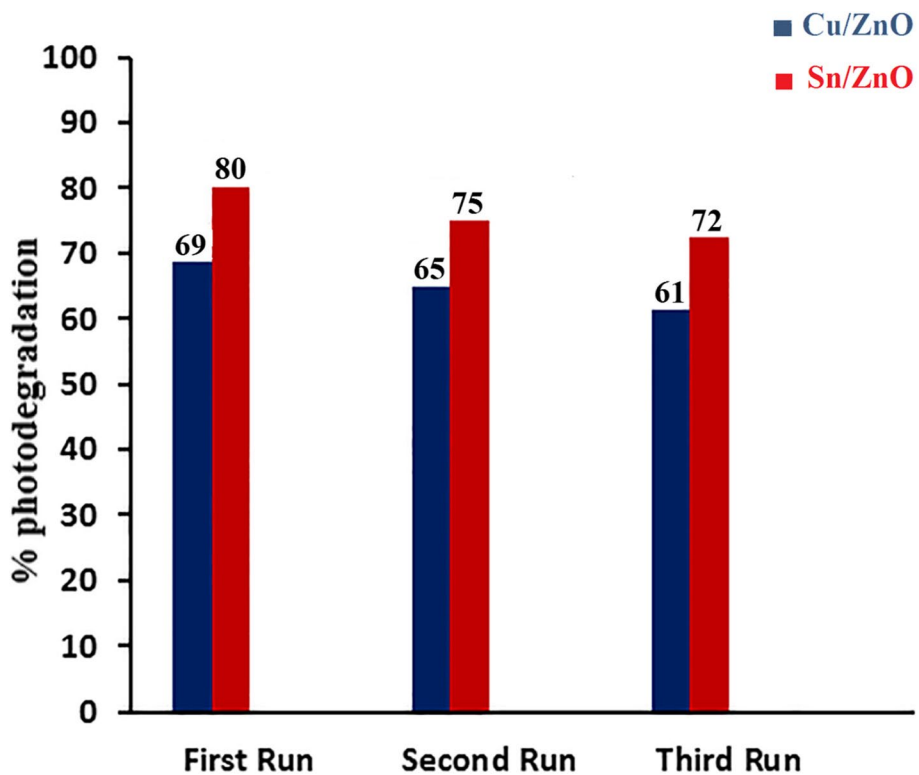

Fig. 8 Photocatalytic degradation percentage of CIT (25 µg mL^{-1}, pH 7) in the presence of Sn/ZnO (0.5 mg mL^{-1}) and CIT (25 µg mL^{-1}, pH 9) in the presence of Cu/ZnO (0.5 mg mL^{-1}) after three successive runs upon exposure to 48 W LED lamp for 2 h

Nazim *et al. Sustainable Environment Research*   (2023) 33:39

Page 15 of 16

high photostability against photocorrosion activity offering an economical advantage.

3.7 Application to incurred samples

CIT initial concentration for incurred samples collected during first wash cycle of the production lines and was 34 µg mL^{-1}. Whereas in the samples collected during second wash CIT initial concentration was found to be 0.9 µg mL^{-1}. A control sample was prepared then doped Sn/ZnO and Cu/ZnO were used for photocatalytic degradation of CIT as a treatment protocol and investigated using first wash samples. Upon using Sn/ZnO, the percentage of degradation was found to be 78 and 77% for the incurred and control samples respectively under the optimum conditions. The absence of significant difference revealed lack of matrix interference. While upon using Cu/ZnO, the percentage of degradation was 68 and 69% for the incurred and control samples respectively. When the treatment protocol was applied to second wash sample, CIT peak was not detected owing to its relatively low concentration (less than the assay LOD). These results showed the efficiency of both Sn/ZnO and Cu/ZnO as photocatalyst in treatment of wastewater collected during CIT cleaning validation with relatively higher photodegradation upon using Sn as a dopant for ZnO NPs.

4 Conclusions

Pure ZnO and Mg, Cu and Sn doped ZnO NPs were synthesized by simple low-cost chemical co-precipitation method using no hazardous chemicals. The NPs showed high crystalline and enhanced optical absorption as confirmed by HR-TEM, XRD and UV-Vis DRS. The optical properties of ZnO was tuned using different metal dopants. The effect of the metal dopants on ZnO photocatalysis was compared. Sn doping showed the highest photocatalytic activity followed by Cu and then Mg upon visible LED irradiation. A percentage degradation of 80% was obtained in 2 h using a low energy household LED lamp upon using Sn/ZnO NPs. Analysis of full factorial design had revealed a significant interaction between metal dopant and pH. Better photocatalytic activity for Sn/ZnO was achieved at pH 7 while optimum pH for Cu/ZnO was at 9, owing to high surface charge and colloidal stability of NPs. The kinetics of CIT photocatalytic degradation was studied using both Sn/ZnO and Cu/ZnO at optimum set of experimental conditions. The rate constant value of Sn/ZnO (0.011 min^{-1}) was approximately two times higher than that of Cu/ZnO (0.0076 min^{-1}) for degradation of CIT. The Sn/ZnO not only showed higher photocatalytic activity, but also exhibited better reusability over three successive cycles. The highly stable and reusable nature of the synthesized Sn/ZnO could be of potential value on industrial application by controlling the economic cost. The treatment protocol was successfully applied for samples collected during the cleaning validation process of CIT production lines. The integration of such cost effective approach into the currently employed cleaning validation protocols would offer a great economical advantage for pharmaceutical wastewater treatment and thus the development of industrial-scale photocatalytic technologies. Results were promising for further development of sustainable environmental remediation technologies, based on solar light as a renewable source of energy.

Supplementary Information

The online version contains supplementary material available at https://doi.org/10.1186/s42834-023-00198-3.

Additional file 1: Table S1. Surface parameters of photocatalysts. **Fig. S1.** Chemical structure of citalopram. **Fig. S2.** CZE electropherogram of (a) CIT sample (50 µg mL^{-1}) not subjected to visible light irradiation. (b) CIT photocatalytic degradation upon exposure to 48 W LED lamp at pH 7 for 2 h in the absence of NP. (c) CIT photocatalytic degradation upon exposure to 48 W LED lamp at pH 7 for 2 h in the presence of 0.5 mg mL^{-1} pure ZnO NP.

Authors' contributions
Veronia S. Nazim: Methodology, Investigation, Formal analysis, Visualization, Writing – original draft. Ghada M. El-Sayed: Supervision, Validation, Resources, Writing – review & editing. Sawsan M. Amer: Conceptualization, Project administration, Supervision. Ahmed H. Nadim: Methodology, Investigation, Data curation, Formal analysis, Validation, Resources, Writing – review & editing.

Availability of data and materials
All data generated or analyzed during this study are included in this paper.

Declarations

Competing interests
The authors declare that they have no known competing financial interests or personal relationships that could have appeared to influence the work reported in this paper.

Author details
[1] Analytical Chemistry Department, Faculty of Pharmacy, Cairo University, Cairo 11562, Egypt.

References

1. Alansi AM, Al-Qunaibit M, Alade IO, Qahtan TF, Saleh TA. Visible-light responsive BiOBr nanoparticles loaded on reduced graphene oxide for photocatalytic degradation of dye. J Mol Liq. 2018;253:297–304.
2. Fadillah G, Saleh TA, Wahyuningsih S, Ninda Karlina Putri E, Febrianastuti S. Electrochemical removal of methylene blue using alginate-modified graphene adsorbents. Chem Eng J. 2019;378:122140.
3. Saleh TA. Nanocomposite of carbon nanotubes/silica nanoparticles and their use for adsorption of Pb(II): from surface properties to sorption mechanism. Desalin Water Treat. 2016;57:10730–44.
4. Koe WS, Lee JW, Chong WC, Pang YL, Sim LC. An overview of photocatalytic degradation: photocatalysts, mechanisms, and development of photocatalytic membrane. Environ Sci Pollut R. 2020;27:2522–65.
5. Mohamed KM, Benitto JJ, Vijaya JJ, Bououdina M. Recent Advances in ZnO-based nanostructures for the photocatalytic degradation of hazardous, non-biodegradable medicines. Crystals. 2023;13:329.
6. Carofiglio M, Barui S, Cauda V, Laurenti M. Doped zinc oxide nanoparticles: synthesis, characterization and potential use in nanomedicine. Appl Sci. 2020;10:5194.
7. Ong CB, Ng LY, Mohammad AW. A review of ZnO nanoparticles as solar photocatalysts: Synthesis, mechanisms and applications. Renew Sust Energ Rev. 2018;81:536–51.
8. Alansi AM, Qahtan TF, Saleh TA. Solar-driven fixation of bismuth oxyhalides on reduced graphene oxide for efficient sunlight-responsive immobilized photocatalytic systems. Adv Mater Interfaces. 2021;8:2001463.
9. Saleh TA. Nanomaterials: Classification, properties, and environmental toxicities. Environ Technol Inno. 2020;20:101067.
10. Saleh TA. Protocols for synthesis of nanomaterials, polymers, and green materials as adsorbents for water treatment technologies. Environ Technol Innov. 2021;24:101821.
11. Balela MDL, Acedera RA, Flores CLI, Pelicano CMO. Surface modification of ZnO nanostructured film prepared by hot water oxidation. Surf Coat Tech. 2018;340:199–209.
12. Sanchez-Cid P, Jaramillo-Paez C, Navio JA, Martin-Gomez AN, Hidalgo MC. Coupling of Ag_2CO_3 to an optimized ZnO photocatalyst: Advantages vs. disadvantages. J Photoch Photobio A. 2019;369:119–32.
13. Jouya M, Taromian F, Afshari Abolkarlou M. Growth of Zn thin films based on electric field by thermal evaporation method and effect of oxidation time on physical properties of ZnO nanorods. J Mater Sci-Mater El. 2020;31:8680–9.
14. Mostafa AM, Mwafy EA. Synthesis of ZnO and Au@ZnO core/shell nanocatalysts by pulsed laser ablation in different liquid media. J Mater Res Technol. 2020;9:3241–8.
15. Jamkhande PG, Ghule NW, Bamer AH, Kalaskar MG. Metal nanoparticles synthesis: An overview on methods of preparation, advantages and disadvantages, and applications. J Drug Deliv Sci Tec. 2019;53:101174.
16. Ahmad I, Akhtar MS, Ahmed E, Ahmad M. Highly efficient visible light driven photocatalytic activity of graphene and CNTs based Mg doped ZnO photocatalysts: A comparative study. Sep Purif Technol. 2020;245:116892.
17. Wang J, Sun XH, Du H. Oxygen defect Sn-doped ZnO nanorods for enhanced photocatalytic activity under visible light irradiation. Russ J Inorg Chem. 2020;65:1111–8.
18. Venkatesh N, Aravindan S, Ramki K, Murugadoss G, Thangamuthu R, Sakthivel P. Sunlight-driven enhanced photocatalytic activity of bandgap narrowing Sn-doped ZnO nanoparticles. Environ Sci Pollut R. 2021;28:16792–803.
19. Adam RE, Alnoor H, Pozina G, Liu X, Willander M, Nur O. Synthesis of Mg-doped ZnO NPs via a chemical low-temperature method and investigation of the efficient photocatalytic activity for the degradation of dyes under solar light. Solid State Sci. 2020;99:106053.
20. Vaiano V, Iervolino G, Rizzo L. Cu-doped ZnO as efficient photocatalyst for the oxidation of arsenite to arsenate under visible light. Appl Catal B-Environ. 2018;238:471–9.
21. Siva N, Sakthi D, Ragupathy S, Arun V, Kannadasan N. Synthesis, structural, optical and photocatalytic behavior of Sn doped ZnO nanoparticles. Mat Sci Eng B-Solid. 2020;253:114497.
22. Andhare DD, Jadhav SA, Khedkar MV, Somvanshi SB, More SD, Jadhav KM. Structural and chemical properties of $ZnFe_2O_4$ nanoparticles synthesised by chemical co-precipitation technique. J Phys Conf Ser. 2020;1644:012014.
23. Saleh TA, Agarwal S, Gupta VK. Synthesis of $MWCNT/MnO_2$ and their application for simultaneous oxidation of arsenite and sorption of arsenate. Appl Catal B-Environ. 2011;106:46–53.
24. Shunmuga Sundaram P, Sangeetha T, Rajakarthihan S, Vijayalaksmi R, Elangovan A, Arivazhagan G. XRD structural studies on cobalt doped zinc oxide nanoparticles synthesized by coprecipitation method: Williamson-Hall and size-strain plot approaches. Physica B. 2020;595:412342.
25. Saleh TA. Carbon nanotube-incorporated alumina as a support for MoNi catalysts for the efficient hydrodesulfurization of thiophenes. Chem Eng J. 2021;404:126987.
26. Ahmed DS, Al-Baidhani M, Adil H, Bufaroosha M, Rashad AA, Zainulabdeen K, et al. Recent study of PF/ZnO nanocomposites: Synthesis, characterization and optical properties. Mater Sci Energ Technol. 2023;6:29–34.
27. Wu G, Wang X, Zhang X, Ren H, Wang Y, Yu Q, et al. Nontarget screening based on molecular networking strategy to identify transformation products of citalopram and sertraline in wastewater. Water Res. 2023;232:119509.
28. Kwon JW, Armbrust KL. Degradation of citalopram by simulated sunlight. Environ Toxicol Chem. 2005;24:1618–23.
29. Sanakousar FM, Vidyasagar CC, Jimenez-Perez VM, Prakash K. Recent progress on visible-light-driven metal and non-metal doped ZnO nanostructures for photocatalytic degradation of organic pollutants. Mat Sci Semicon Proc. 2022;140:106390.
30. Lu J, Batjikh I, Hurh J, Han Y, Ali H, Mathiyalagan R, et al. Photocatalytic degradation of methylene blue using biosynthesized zinc oxide nanoparticles from bark extract of *Kalopanax septemlobus*. Optik. 2019;182:980–5.
31. Nazim VS, El-Sayed GM, Amer SM, Nadim AH. Functionalized SnO_2 nanoparticles with gallic acid via green chemical approach for enhanced photocatalytic degradation of citalopram: synthesis, characterization and application to pharmaceutical wastewater treatment. Environ Sci Pollut R. 2023;30:4346–58.
32. Bojanowska-Czajka A, Pyszynska M, Majkowska-Pilip A, Wawrowicz K. Degradation of selected antidepressants sertraline and citalopram in ultrapure water and surface water using gamma radiation. Processes. 2022;10:63.
33. Chandekar KV, Shkir M, Al-Shehri BM, AlFaify S, Halor RG, Khan A, et al. Visible light sensitive Cu doped ZnO: Facile synthesis, characterization and high photocatalytic response. Mater Charact. 2020;165:110387.
34. Vallejo W, Cantillo A, Diaz-Uribe C. Methylene blue photodegradation under visible irradiation on Ag-doped ZnO thin films. Int J Photoenergy. 2020;2020:1627498.
35. Nguyen LTT, Nguyen LTH, Duong ATT, Nguyen BD, Quang Hai N, Chu VH, et al. Preparation, characterization and photocatalytic activity of La-doped zinc oxide nanoparticles. Materials. 2019;12:1195.
36. Shirdel B, Behnajady MA. Visible-light-induced degradation of Rhodamine B by Ba doped ZnO nanoparticles. J Mol Liq. 2020;315:113633.
37. Hanh NT, Le Minh Tri N, Van Thuan D, Thanh Tung MH, Pham TD, Minh TD, et al. Monocrotophos pesticide effectively removed by novel visible light driven Cu doped ZnO photocatalyst. J Photoch Photobio A. 2019;382:111923.
38. Peter CN, Anku WW, Sharma R, Joshi GM, Shukla SK, Govender PP. N-doped ZnO/graphene oxide: a photostable photocatalyst for improved mineralization and photodegradation of organic dye under visible light. Ionics. 2019;25:327–39.
39. Alakhras F, Alhajri E, Haounati R, Ouachtak H, Addi AA, Saleh TA. A comparative study of photocatalytic degradation of Rhodamine B using natural-based zeolite composites. Surf Interfaces. 2020;20:100611.